A High-Quality Rectifier Based on the Forward Topology With Secondary-Side Resonant Reset

Giorgio Spiazzi, *Member, IEEE*

***Abstract*—The use of buck-derived topologies for unity power factor ac-to-dc applications is limited by their inherent inability to draw current from the line in those intervals, during the line half period, in which the input voltage is lower than the output one.**

This drawback is overcome in the proposed high-quality rectifier based on the forward topology with secondary-side resonant reset. The employed secondary side reset capacitor is able to provide proper transformer reset by recycling the transformer stored energy to the load and, at the same time, it allows to draw energy from the line even when the input voltage is lower than the output one. Consequently, besides to a better utilization of the transformer core (bipolar core excitation), a low distorted input current waveform can be obtained with a power factor close to unity.

Experimental results of a 200 W prototype confirm the theoretical expectations.

***Index Terms*—Bipolar core excitation, buck-derived topologies, capacitor, input voltage, transformer core.**

I. Introduction

THE FIELD of power factor correctors (PFCs), i.e., rectifiers that draw a current from the line proportional to the input voltage (unity power factor), is almost totally dominated by the boost and the flyback topologies. Boost rectifiers provide an inherent input current filtering but they lack of an overcurrent protection and they require an output voltage greater than the line voltage peak [1]. Moreover, isolated boost structures are complicated [2]. On the other hand, in low power applications requiring isolation, the flyback topology represents the best choice due to its simplicity [3]. However, the unavoidable transformer leakage inductance calls for heavy snubbering in order to control the switch overvoltage and the electromagnetic noise generated (EMI).

Rectifiers based on buck-derived topologies are not widely used mainly for their inability to draw current from the line in those interval, during the line half period, in which the rectified input voltage is lower than the output one, since they can operate only as step-down regulators [4], [5].

This problem can be overcome by using a suitable secondary-side resonant reset scheme, in conjunction with the forward topology, which ensures proper transformer reset, while providing the boost action necessary to draw current from the line in the whole line half period. The result is a rectifier with a power factor close to unity, which provides isolation, with a good transformer utilization (bipolar core excitation), with only one switch and with less transformer leakage inductance problems as compared to the flyback topology.

Manuscript received July 10, 2000; revised November 1, 2001. This paper was presented at the 31st Annual IEEE Power Electronics Specialists Conference, Galway, Ireland, June 18–23, 2000. Recommended by Associate Editor T. Sloane.

The author is with the Department of Information Engineering (DEI), University of Padova, Padova 35131, Italy (e-mail: giorgio.spiazzi@unipd.it).

Digital Object Identifier 10.1109/TPEL.2003.810843

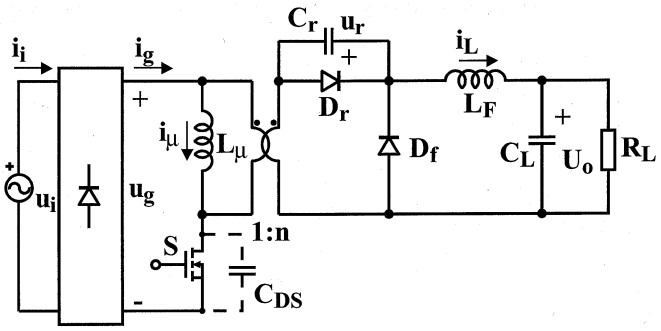

Fig. 1. Scheme of the proposed high-quality rectifier based on a forward converter with secondary-side resonant reset.

In Sections II and III the converter analysis is reported for both step-down and step-up modes considering a constant input voltage, while Section IV describes the application of the converter as a high quality rectifier. Finally, results of an experimental prototype are reported confirming the theoretical expectations.

II. Converter Analysis in Step-Down Mode

The proposed high-quality rectifier based on the forward topology is shown in Fig. 1. As we can see, the secondary-side resonant reset scheme is simply made up by capacitor C_r connected in parallel with the rectifier diode D_r. The transformer reset occurs through the resonance between its magnetizing inductance L_μ and the resonant capacitor C_r during the switch off-time, and the mechanism is conceptually equal to the standard resonant reset scheme which exploit the switch output capacitance C_{DS} (shown with a dotted line in Fig. 1) [6]. The only difference is that the transformer-stored energy can now be partially delivered to the load instead of being dissipated in the switch at turn on.

In order to keep the notation simple, a constant input voltage U_g is considered and the extension to rectifier operation is considered in Section IV.

In general, the converter can operate in different modes characterized by different topological sequences in a switching period: all these possible sub topologies are shown in Fig. 2, from $T1$ to $T6$ (there are three devices each of them having two possible states for a total of eight different combinations, but the two corresponding to $S = D_f =$ "ON" are not allowed).

We will analyze first the normal step-down operation ($U_g > U_{op}$ where U_{op} is the output voltage reflected to the primary

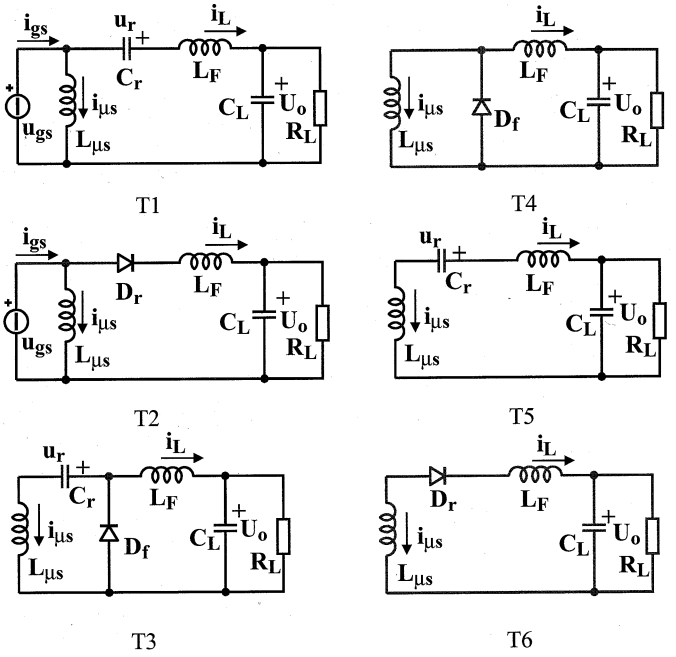

Fig. 2. Converter sub topologies in a switching period (NOTE: u_{gs}, i_{gs}, $L_{\mu s}$, $i_{\mu s}$ are variables referred to the transformer secondary side.)

side), in which the converter behaves very similar to a standard forward converter. Assuming a continuous conduction mode (CCM) of operation (i.e., the freewheeling diode remains on during the whole switch off-time), the converter can assume only two operating modes $M0$ and $M1$, described by the waveforms shown in Fig. 3. These operating modes are characterized by the following topological sequences in each switching period:

$$M0\text{: } T1 \rightarrow T2 \rightarrow T3$$

$$M1\text{: } T2 \rightarrow T3 \rightarrow T4$$

and are described hereafter. In the following analysis, a load current much higher then the magnetizing one reflected to the secondary side is assumed ($i_L > i_\mu/n$ where $n = N_2/N_1$ is the transformer turns ratio). Moreover, the output current ripple is neglected, so that $i_L = I_L = I_o$.

A. Mode $M0$

This operating mode occurs when the switch off-time is shorter than one half of the resonant period, so that the resonant capacitor C_r is not completely discharged during the switch turn off interval. For a better understanding of the converter operation let us refer to Fig. 3, which reports the converter main waveforms in a switching period.

Interval $T_{02} = t_2 - t_0 = dT_s$. At instant t_0 the switch is turned on causing the turn off of the freewheeling diode D_f. During the first interval $T_{01} = t_1 - t_0$, diode D_r remains off (see Fig. 2-$T1$) until capacitor C_r is completely discharged by the filter inductor current (instant t_1)

$$u_r(t) = U_{r0} - \frac{I_L}{C_r}t \quad T_{01} = \frac{U_{r0}C_r}{I_L} \tag{1}$$

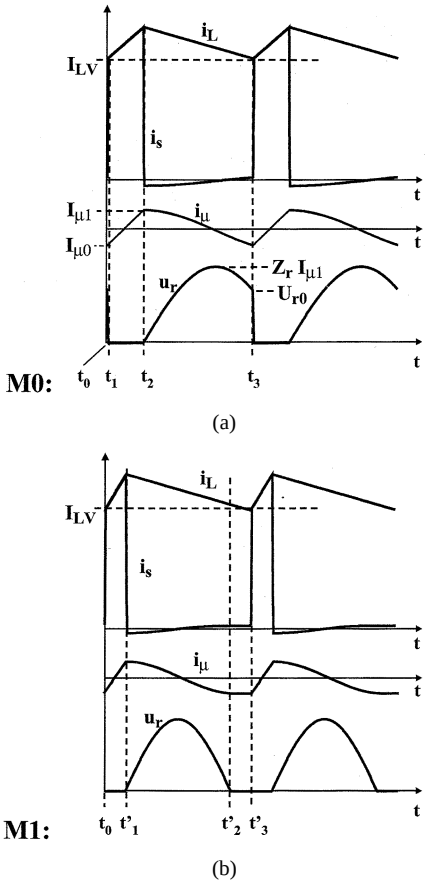

Fig. 3. Converter main waveforms corresponding to operating modes $M0$ and $M1$ in a switching period ($T_s = t_3 - t_0 = t'_3 - t_0$).

where U_{r0} is the initial capacitor voltage value. During this interval, the energy stored in C_r is delivered to the load. After instant t_1, the topology changes as shown in Fig. 2-$T2$, becoming the standard powering phase of the forward converter.

At the same time, the magnetizing current starts to increase linearly at the switch turn on until instant t_2, i.e., ($I_{\mu 0}$ is the initial value)

$$i_\mu(t) = I_{\mu 0} + \frac{U_g}{L_\mu}t. \tag{2}$$

Interval $T_{23} = t_3 - t_2 = (1-d)T_s$. At instant t_2 the switch is turned off and diode D_f starts to conduct. The magnetizing current transfers to the secondary winding and charges, in a resonant way, the reset capacitor C_r (see Fig. 2-$T3$). On the assumption of a load current much higher then the magnetizing one, current i_μ can reverse, with D_f still on ($i_{Df} = i_\mu/n + i_L$). During this subinterval, the resonant waveforms are given by (a new time origin is assumed in t_2)

$$\begin{aligned} u_r(t') &= Z_r I_{\mu 1} \sin(\omega_r t') \\ i_\mu(t') &= I_{\mu 1} \cos(\omega_r t') \end{aligned} \tag{3}$$

where

$$I_{\mu 1} = I_{\mu 0} + \frac{U_g}{L_\mu}dT_s \tag{4}$$

is the peak magnetizing current and

$$\omega_r = \frac{1}{n\sqrt{L_\mu C_r}}, \quad Z_r = \sqrt{\frac{L_\mu}{C_r}} \tag{5}$$

are the resonant tank parameters. At the end of the off interval, under a steady state condition, we can write

$$\begin{aligned} u_r(T_{off}) &= Z_r I_{\mu 1} \sin(\omega_r T_{off}) = U_{r0} \\ i_\mu(T_{off}) &= I_{\mu 1} \cos(\omega_r T_{off}) = I_{\mu 0}. \end{aligned} \tag{6}$$

From (4)–(6), the initial magnetizing current value $I_{\mu 0}$ results

$$I_{\mu 0} = -\frac{U_g}{2L_\mu} dT_s \gamma$$

$$\gamma = \begin{cases} \dfrac{-2\cos(\omega_r(1-d)T_s)}{1-\cos(\omega_r(1-d)T_s)} & \omega_r(1-d)T_s < \pi \\ 1 & \omega_r(1-d)T_s > \pi \end{cases} \tag{7}$$

where the parameter γ assumes values lower than one for operating mode $M0$, and is equal to one for operating mode $M1$. The magnetizing peak current is given by

$$I_{\mu 1} = \frac{U_g}{2L_\mu} dT_s (2-\gamma) \tag{8}$$

while the average value is

$$I_{\mu avg} = \frac{U_g}{2L_\mu} dT_s (1-\gamma). \tag{9}$$

Note that, $I_{\mu 1}$ is constant and equal to $-I_{\mu 0}$ during mode $M1$ (the core excitation is symmetrical with zero average value) and increases as the converter enters mode $M0$, since γ becomes lower than one. In the latter case the magnetizing current acquires a positive average value, as can be inferred from (9). It is this shift of the transformer flux, which gives, to this operating mode, a certain degree of boost effect. In fact, part of the magnetic energy stored in the transformer during the switch on-time is transferred to the resonant capacitor C_r during the turn off interval, and then to the load during interval T_{01}. This can be demonstrated by finding an approximate expression for the voltage conversion ratio during mode $M0$. This can be done by observing that the output voltage is always given by the average value of the voltage across the freewheeling diode, i.e.

$$U_o = nU_g d + \frac{T_{01}}{2T_s} U_{r0}. \tag{10}$$

In (10), the second term reflects the average value of voltage $u_r(t)$, given by (1), during interval T_{01}, since the freewheeling diode voltage u_{Df} equals $nU_g + u_r$ during the switch off interval. Now using (1)–(6) we obtain

$$M = d \cdot F(d, k)$$

$$F(d, k) = \frac{1}{2}\left[1 + \sqrt{1 + \frac{4}{k}\left(\frac{1+\cos(\omega_r(1-d)T_s)}{1-\cos(\omega_r(1-d)T_s)}\right)}\right] \tag{11}$$

where $k = (2L_\mu f_s n^2)/R_L$ is an adimensional parameter usually found in converters operating in discontinuous mode.

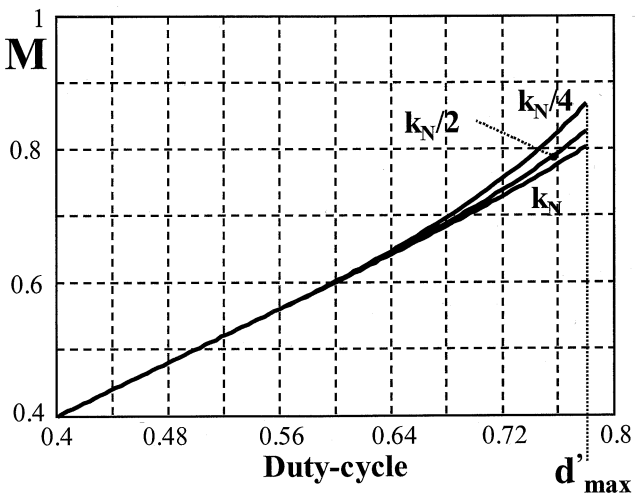

Fig. 4. Voltage conversion ratio as a function of duty-cycle for different k values (k_N corresponds to the nominal load resistance).

Let us show the boost effect with the following example: $U_g = 30 \div 60$ V, $U_o = 48$ V, $I_o = 4$ A, $n = 2$, $f_s = 50$ kHz, $L_\mu = 1$ mH, $C_r = 2$ nF. With the constraint of $I_{\mu 0} \leq 0$ (it is an arbitrary design choice to limit the maximum flux in the transformer), the maximum boost effect, needed at minimum input voltage, is achieved when the condition $T_r/4 = T_{off}$ is met. In fact the energy stored in capacitor C_r and delivered to the load during interval T_{01} is given by

$$E_r = \frac{1}{2} C_r U_{r0}^2 = \frac{U_g^2}{2L_\mu} (dT_S)^2 \frac{1}{tg^2\left(\frac{\omega_r(1-d)T_S}{2}\right)}. \tag{12}$$

This energy reaches the maximum value of $E_{rMAX} = (U_g^2/2L_\mu)(dT_S)^2$ when $\omega_r(1-d)T_S = \pi/2$ and $I_{\mu 0} = 0$. Based on these considerations, the resonant capacitor value was chosen in order to satisfy the following constraint:

$$f_r = \frac{f_s}{4(1-d'_{\max})} \tag{13}$$

where $d'_{\max}$ is the maximum duty-cycle needed to obtain the desired output voltage in correspondence to the minimum input voltage, taking into account the boost effect.

Fig. 4 reports the actual voltage conversion ratio M as the function of duty-cycle for three different k values (k_N is the value of k corresponding to the nominal load resistance): as we can see, the boost action starts above $d \approx 0.6$ and increases as the load current decreases. However, this effect vanishes at higher magnetizing inductance values [see eq. (12)], thus reducing the energy transferred to the load.

B. Mode $M1$

If the resonant period $T_r = 2\pi/\omega_r$ is shorter than $2T_{off}$, then the converter waveforms modify as shown in Fig. 3-$M1$, i.e., a complete half resonance occurs during the switch off time. Since voltage u_r cannot reverse, at instant t'_2 it goes to zero and remains zero, while the magnetizing current continues to flow through D_r and D_f (see Fig. 2-$T4$). As a consequence, the initial voltage U_{r0} across C_r is zero and $I_{\mu 0} = -I_{\mu 1}$. Clearly, this

operating mode corresponds to a standard forward operation, in which only the reset mechanism is modified.

Before to end the analysis of the converter in step-down mode, it is interesting to show the effect of the selection of the resonant capacitor C_r on the maximum switch voltage stress. To this purpose, we are going to compare two different choices:

a) C_r is selected in order to satisfy condition (13) so as to exploit the maximum boost effect of mode $M0$;
b) C_r is selected in order to operate at the boundary between modes $M0$ and $M1$ at the minimum input voltage, i.e., according to the following condition:

$$f_r = \frac{f_s}{2\,(1 - d_{\max})} \tag{14}$$

where $d_{\max} = U_o/nU_{g\min} = 0.8 > d'_{\max}$. In this case the converter behaves as a standard forward one, without any boost effect, because it continues to operate in Mode $M1$ also at higher input voltages (lower duty-cycles).

In case of solution b), assuming a continuous conduction mode, the converter operates always in Mode $M1$, the parameter γ is equal to one and the peak voltage across the resonant capacitor remains constant and equal to [using (5), (6), (8), (14)]

$$\hat{U}_{rM1} = Z_r I_{\mu 1} = U_o \pi \frac{f_r}{f_s} = U_o \frac{\pi}{2} \frac{1}{1 - d_{\max}}. \tag{15}$$

On the other hand, with solution a), at minimum input voltage the maximum duty-cycle $d'_{\max}$ turns out to be 0.78, thanks to the boost action (see Fig. 4). Consequently, the resonant capacitor peak voltage reaches the maximum value at the minimum input voltage, since the magnetizing current reaches its maximum value [given by (8) for $U_{g\min}$, $d'_{\max}$, and $\gamma = 0$], and reduces at lower duty-cycle values (higher input voltages) because $I_{\mu 1}$ decreases. In both cases, the switch voltage stress is given by

$$\hat{U}_{sw} = U_g + \frac{\hat{U}_r}{n}. \tag{16}$$

Fig. 5 shows the comparison between the two design approaches: as we can see, exploiting the boost effect gives a considerable benefit in terms of maximum switch voltage stress, and it is the preferred choice also for rectifier operation, as it will be shown later. This advantage is counterbalanced by a maximum flux in the core which is twice the flux we had selecting C_r based on criterion b), because, in the latter case, the magnetizing current is always symmetric with zero average value.

III. Converter Analysis in Step-Up Mode

When the input voltage is lower than the output voltage reflected to the primary side, the proposed converter is able to operate in different modes, depending on converter parameter values and duty-cycle. In the following, we will illustrate two of them that appear at low input voltage and load current, which correspond exactly to the situation encountered in a high power factor rectifier around the zero crossing of the line voltage.

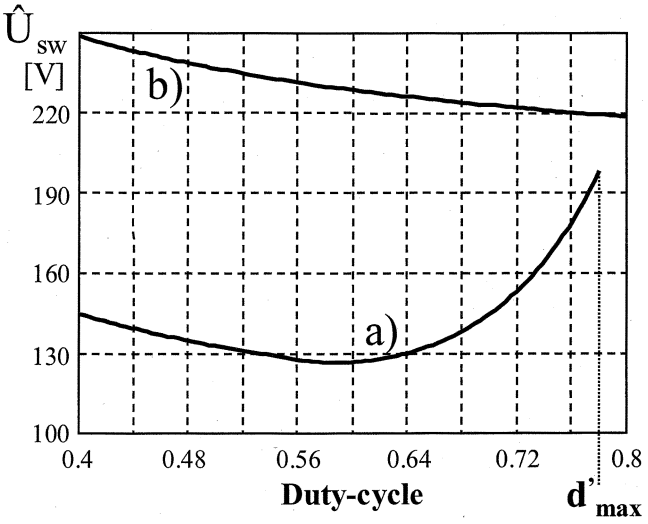

Fig. 5. Switch voltage stress as a function of duty-cycle for two different design approaches: (a) f_r is chosen according to (13) and (b) f_r is chosen according to (14).

The converter main waveforms describing these two operating modes are reported in Fig. 6 and the corresponding topological sequences are

$$\text{Mode } M2\text{: } T1 - T3 - T5$$

$$\text{Mode } M3\text{: } T1 - T2 - T3 - T5.$$

These waveforms were obtained by simulation of a rectifier having the following parameters $U_g = 230$ V_{rms}, $U_o = 160$ V, $P_o = 600$ W, $n = 1$, $f_s = 50$ kHz, $L_\mu = 2$ mH, $C_r = 10$ nF, $L_F = 450$ μH. In particular, the waveforms corresponding to mode $M2$ and $M3$ were recorded after 0.5 ms and 1 ms from the line voltage zero crossing, respectively (the line frequency was 50 Hz).

Mode $M2$. Starting from the turn on of the switch at instant t_0, the magnetizing current increases linearly while the filter inductance L_F resonates with capacitor C_r accumulating the energy previously stored in the resonant capacitor. The corresponding sub topology is shown in Fig. 2-$T1$. At instant t_1, the switch is turned off causing the turn on of the freewheeling diode D_f (see Fig. 2-$T3$): the magnetizing inductance resonates with C_r while the filter inductor current decreases linearly until it becomes equal to $-i_{\mu s}$ (the magnetizing current value reflected to the secondary side). This occurs at instant t_2, thus causing the turn off of D_f: from now until the subsequent switching interval, C_r resonates with the sum of $L_{\mu s}$ (the magnetizing inductance reflected to the transformer secondary side) and L_F (see Fig. 2-$T5$).

Mode $M3$. This mode of operation differs from the previous one because during the switch on time the resonant capacitor C_r discharges to zero (instant t_1), causing the turn on of diode D_r (see Fig. 2-$T2$). During the corresponding subinterval [t_1, t_2], the magnetizing current continues to increase linearly while the filter inductance L_F discharges to the load (note the negative slope of current i_L caused by an input voltage u_{gs} lower than the output one). When the switch turns off the topological sequence is the same of the previous mode $M2$.

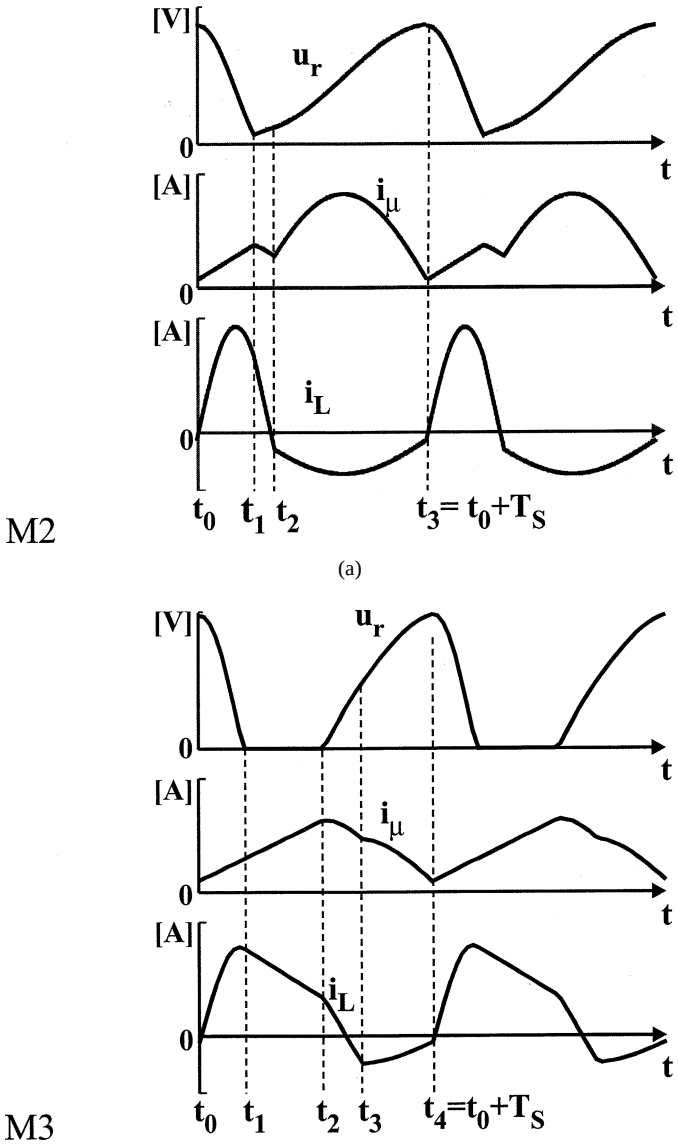

Fig. 6. Converter main waveforms corresponding to the operating modes: (a) $M2$ and (b) $M3$.

From the waveforms of Fig. 6-$M2$ and $M3$, we can see that during the switch on-time the input current $i_g = i_\mu + n \cdot i_L$ is positive, i.e., energy is transferred from the line to the load even when the input voltage is lower than the reflected output one. Actually, in mode $M2$ the instantaneous voltage conversion ratio was 3.1, while during mode $M3$ was 1.6. This, represents a stronger boost effect, as compared to that encountered in mode $M0$, and it allows to overcome the inherent inability of buck-type rectifiers of drawing current from the line in the intervals corresponding to an instantaneous input voltage lower than the reflected output one.

IV. Analysis of the Converter as High-Quality Rectifier

When the converter operates as a high-quality rectifier, the voltage conversion ratio and the apparent load seen by the converter changes during the line angle $\theta = \omega t$, i.e., assuming a unity power factor we can write [7]

$$m(\theta) = \frac{U_o}{n\hat{U}_i |\sin(\theta)|} = \frac{M}{|\sin(\theta)|} \tag{17}$$

$$r_L(\theta) = \frac{R_L}{2\sin^2(\theta)}. \tag{18}$$

Thus, a high boost capability is required around the line voltage zero crossing, but with a load current which is very small as compared to the average value. Standard buck-type rectifiers, being able of a step-down action only, have a non zero input current only during a portion of the line half period [4], [5], i.e., for $\theta_d < \theta < \pi - \theta_d$, where

$$\theta_d = \sin^{-1}\left(\frac{U_o}{n\hat{U}_i}\right) \tag{19}$$

is the dead angle. On the other hand, the proposed rectifier allows overcoming this limitation, as demonstrated in the previous section. In order to verify the theoretical forecasts, a converter simulation was performed using the same parameters employed to derive the waveforms for modes $M2$ and $M3$, which are listed at the beginning of Section III. The filtered input current waveform results as shown in Fig. 7. Charge control was employed to force the average input current to follow a suitable sinusoidal reference waveform, i.e., the switch current is integrated cycle by cycle and the result is compared to the sinusoidal reference in order to determine the switch turn off instant [3]. As we can see, the converter draws current from the grid in the whole line period, while the dead angle given by (19) is 30°. The small current distortion at the line voltage zero crossing is due to the stabilizing ramp added to the controlled signal needed to avoid the inherent instability of the charge control (similar to the peak current control instability).

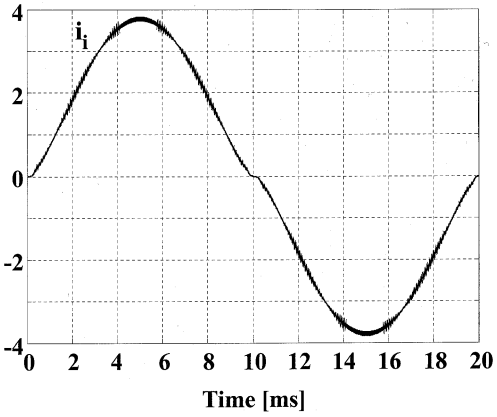

Fig. 7. Simulated filtered input current waveform of proposed forward rectifier with charge control.

For θ ranging from 0 to $\pi/2$, the converter passes through the following operating modes (at instants 0.5ms and 2ms respectively): $M2 \rightarrow M3 \rightarrow M0$.

The simulated magnetizing current i_μ and switch voltage u_{DS} are shown in Fig. 8 in the first 90° of the line angle: it is important to note that the switch voltage stress occurs at the peak of the line voltage, and the magnetizing peak current changes very little during the line period. In other words,

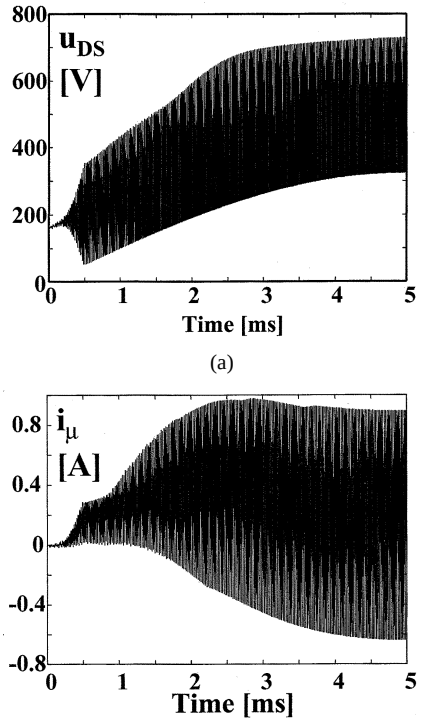

Fig. 8. Simulated switch voltage and magnetizing current in the first 90° of the line angle (charge control).

TABLE I
CONVERTER PARAMETERS

U_i = 90-260 V_{rms}	U_o = 48 V	P_o = 200 W
n = 0.56	f_S = 56 kHz	C_L = 4400 μF
L_μ = 3.5 mH	C_r = 10 nF	L_F = 300 μH

for a properly designed converter, the boost effect does not increase the device stresses. Thus, the transformer can be designed as in a standard forward converter, considering the volts·second across the winding. The only thing we need is a proper magnetizing inductance value, which can be obtained with a suitable air gap.

V. EXPERIMENTAL RESULTS

A 200 W forward rectifier was built and tested in order to verify the theoretical expectation. The converter parameters are listed in Table I.

The transformer core was ferrite E 42-21-20 with a small air gap in the center lag. The adopted control technique was the modified non linear carrier control described in [8]–[10], which does not require input voltage sensing and current error amplifier as well as any compensation ramp for stability purposes. Its principle scheme is shown in Fig. 9: the switch current is sensed (R_S is the equivalent sensing resistance) and integrated together with the output U_m of the voltage error amplifier; the integrator output is then compared with U_m to determine the turn-off instant. An internal clock sets the switching frequency, turning on the switch at constant intervals. For more details see [8]–[10].

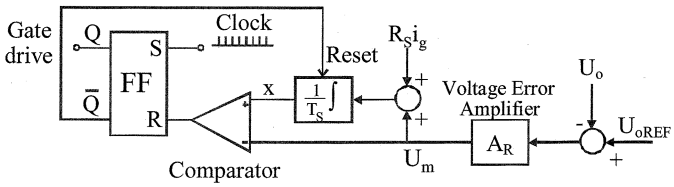

Fig. 9. Simplified scheme of the adopted modified nonlinear carrier control [8]–[10].

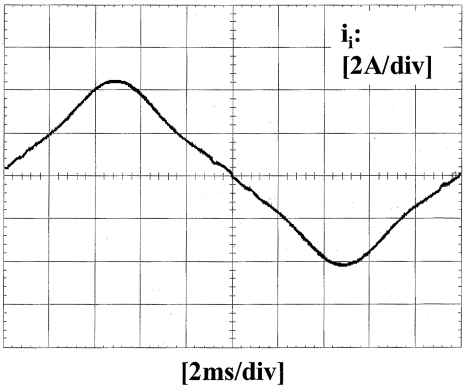

Fig. 10. Filtered input current i_i with modified non linear carrier control ($U_o = 48$ V, $P_o = 200$ W, $U_i = 90$ V_{rms}).

TABLE II
INPUT CURRENT HARMONICS ($U_i = 230$ V_{rms}, $P_o = 200$ W)

Harmonic order	Harmonics [mA_{rms}]	IEC 1000-3-2 [mA_{rms}]
1	977	
3	209	2300
5	26	1440
7	15	770
9	9	400
11	14	330

The filtered input current is shown in Fig. 10 at minimum RMS input voltage: as we can see, the converter was able to draw current in the whole line period as predicted [at the minimum input voltage the dead angle θ_d given by (19) is about 42°]. The low frequency distortion is due to the adopted control scheme, which is best suited for flyback-type rectifiers. Nevertheless, due to the low output power, there is no problem in satisfying the limits imposed by the standard EN 61000-3-2 (Class A piece of equipment), as can be seen from the comparison between the input current harmonics and their limits reported in Table II ($U_i = 230$ V_{rms}, $P_o = 200$ W). Higher order harmonics are negligible, and were not reported in Table II.

Finally, the switch drain-to-source voltage recorded at the line voltage peak is shown in Fig. 11 in two different conditions: a) at the minimum input voltage $U_i = 90$ V_{rms}; b) at the maximum

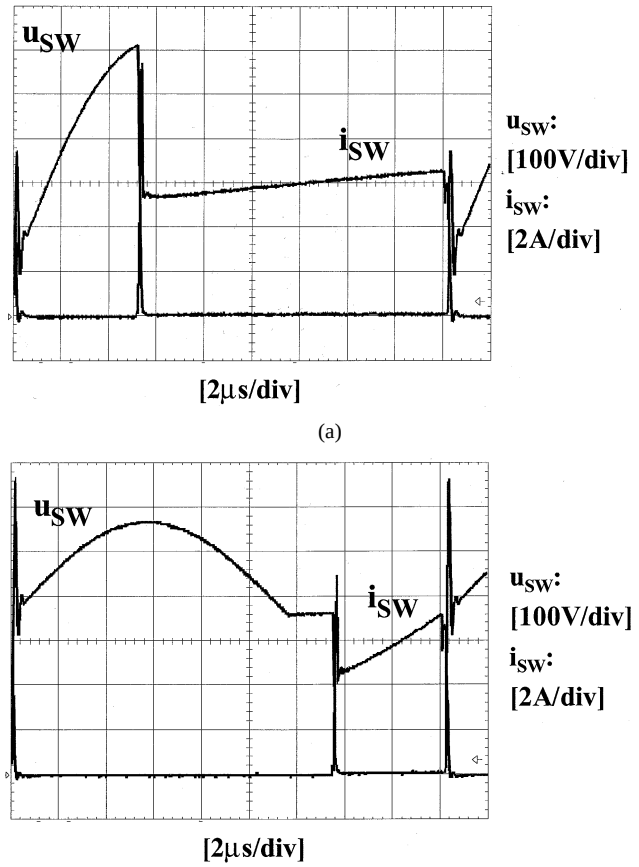

Fig. 11. Measured switch voltage u_{SW} and current i_{SW} recorded at the line voltage peak ($U_o = 48$ V, $P_o = 200$ W): (a) $U_i = 90$ V_{rms} and (b) $U_i = 260$ V_{rms}.

input voltage $U_i = 260$ V_{rms}. As we can see the resonant capacitor C_r was selected according to criterion a) of Section II, so as to fully exploit the boost effect, and the switch voltage stress remains below 750 V in all operating conditions. Note that two small R–C snubbers were used, the first in parallel to the switch ($R_{d1} = 110\ \Omega$, $C_{d1} = 0.5$ nF) and the other in parallel to the transformer secondary winding ($R_{d2} = 75\ \Omega$, $C_{d2} = 0.47$ nF), in order to damp the parasitic oscillations caused by the transformer leakage inductance. From Fig. 11, we can also see that at the line voltage peak the converter operating mode is $M0$ at minimum input voltage and $M1$ at maximum input voltage.

The overall converter efficiency, including also the control losses, is reported in Fig. 12:

a) as a function of input RMS voltage at nominal output power;
b) as a function of output power for different input voltage RMS values.

Due to the design choice, at minimum input voltage the residual voltage across the resonant capacitor C_r at beginning of the switch on time is maximum [see Fig. 11(a)], in order to obtain the maximum boost action. This causes a high voltage stress in the freewheeling diode, with consequent worsening of its reverse recovery behavior. This explains the efficiency reduction at minimum input voltage, as can be seen from Fig. 12: at

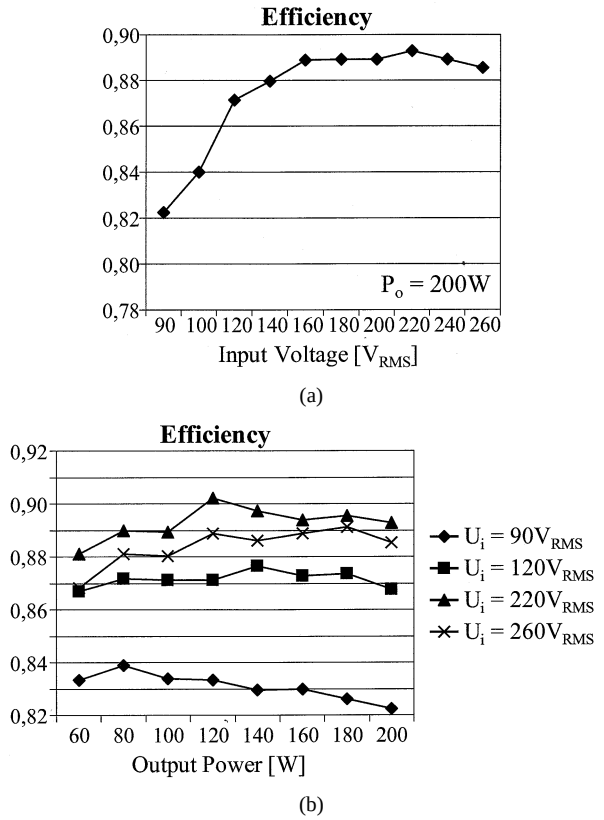

Fig. 12. Measured overall efficiency: (a) as a function of input voltage for nominal power and (b) as a function of output power for different input voltage RMS values ($U_o = 48$ V, $P_o = 200$ W).

higher input voltages, however, the efficiency is good, reaching its maximum around 220 V_{RMS}.

VI. Conclusion

This paper presents a high quality rectifier based on the forward topology. The particular transformer reset mechanism which exploits the resonance between the magnetizing inductance and a secondary-side capacitor, adds a boost effect to the converter, which allows to draw current from the line also in those intervals, during the line half period, in which the rectified input voltage is lower than the reflected output one. The result is an almost unity power factor isolated rectifier with no need of any auxiliary winding for the transformer reset and with a good transformer core utilization (bipolar excitation).

Experimental results of a 200 W prototype confirm the theoretical expectations.

References

[1] C. Zhou and M. Jovanovic, "Design trade-offs in continuous current-mode controlled boost power-factor correction circuits," in *Proc. HFPC Conf.*, 1992, pp. 209–220.
[2] N. Fröhleke, R. Mende, H. Grotstollen, B. Margaritis, and L. Vollmer, "Isolated boost fullbridge topology suitable for high power and power factor correction," in *Proc. IECON'95 Conf.*, 1995, pp. 405–409.
[3] W. Tang, Y. Jiang, G. C. Hua, and F. C. Lee, "Power factor correction with flyback converter employing charge control," in *Proc. APEC Conf.*, 1993, pp. 293–298.
[4] G. Spiazzi, "Analysis of buck converters used as power factor preregulators," in *Proc. IEEE PESC Conf.*, 1997, pp. 564–570.

[5] G. Spiazzi and S. Buso, "Power factor preregulators based on combined buck-flyback topologies," *IEEE Trans. Power Electron.*, vol. 15, pp. 197–204, Mar. 2000.
[6] Cobos, P. Alou, O. Garcia, R. Prieto, J. Uceda, and M. Rascon, "Several alternatives for low output voltage on board converters," in *Proc. IEEE Appl. Power Electron. Conf.*, Feb. 1998, pp. 163–169.
[7] S. D. Freeland, "Input-current shaping for single-phase ac/dc power converters," Ph.D. dissertation, Caltech, Pasadena, CA, 1988.
[8] J. P. Gegner and C. Q. Lee, "Linear peak current mode control: A simple active power factor correction control technique for continuous conduction mode," in *Proc. PESC Conf.*, 1996, pp. 196–202.
[9] Z. Lai and K. Smedley, "A family of power-factor-correction controllers," in *Proc. APEC Conf.*, 1997, pp. 66–73.
[10] G. Spiazzi, S. Buso, and D. Tagliavia, "Simplified control technique for high-power-factor flyback cuk and sepic rectifiers operating in CCM," *IEEE Trans. Ind. Applicat.*, vol. 36, pp. 1413–1418, Sept./Oct. 2000.

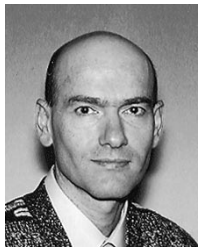

Giorgio Spiazzi (S'92–M'95) was born in Legnago, Verona, Italy, in 1962. He received the M.S. degree (with honors) in electronic engineering and the Ph.D. degree in industrial electronics and informatics from the University of Padova, Padova, Italy, in 1988 and 1993, respectively.

He is an Associate Professor in the Department of Information Engineering, University of Padova. His main research interests are in the fields of advanced control techniques of dc/dc converters, power factor correctors, soft-switching techniques, and electromagnetic compatibility in power electronics.